energy&fuels

Article

pubs.acs.org/EF

# Adsorption Kinetics and Thermodynamics of Vanadyl Etioporphyrin on Asphaltene in Pentane

Feifei Chen, Qingjing Liu, Zhiming Xu, Xuewen Sun, Quan Shi, and Suoqi Zhao*

State Key Laboratory of Heavy Oil Processing, China University of Petroleum, Beijing 102249, People's Republic of China

**ABSTRACT:** The interaction between vanadyl porphyrins and asphaltene in alkane solvents is important to increase the removal rate of metals during the solvent deasphalting process. Thus, the adsorption kinetics and thermodynamics of vanadyl etioporphyrins on a Canadian oil sands bitumen vacuum tower bottom (VTB) asphaltene in *n*-pentane were investigated. After adsorption, asphaltene was analyzed via transmission electron microscopy (TEM), Brunauer–Emmett–Teller (BET), and Fourier transform ion cyclotron resonance mass spectrometry (FT-ICR MS). A certain amount of vanadyl porphyrins was adsorbed by the VTB asphaltene. This adsorption process was affected by the asphaltene dosage (0.01 and 0.02 g), the concentration of the *n*-pentane solution containing vanadyl porphyrins (10 and 15 $\mu$g/mL), and the temperature (288, 293, and 298 K). The adsorption rate was initially distinctly high. However, this rate became much slower after around 300 min, until equilibrium was reached after 1800 min. A comparison of four kinetic models of the overall adsorption rate showed that the adsorption process can be well-described by a pseudo-first-order equation. Furthermore, the adsorption equilibrium fit the Freundlich isotherm. The $\Delta G^\circ$ and $\Delta H^\circ$ values of the adsorption process between vanadyl porphyrins and asphaltenes had been regressed at different temperatures. The absolute value of $\Delta G^\circ$ was less than 20 kJ/mol, whereas that of $\Delta H^\circ$ was greater than 40 kJ/mol.

## INTRODUCTION

Feedstocks of inferior quality and increased metal element content (e.g., nickel and vanadium) are challenges of heavy petroleum upgrading. Previous studies have reported that most of the nickel or vanadium atoms are located in the metal porphyrin structure. However, evidence of the existence of metallic nonporphyrin compounds in heavy petroleum still lacks substantial evidence.[1−4] These metallic compounds are responsible for catalysis deactivation during catalytic cracking, hydrocracking, and bed plugging, which causes light oil yield reduction and poor product quality. Consequently, the removal of metallic compounds has become a concern in several aspects of petroleum upgrading.

Solvent deasphalting can remove contaminants from feedstock, such as asphaltene and metallic compounds, and improve the processability of deasphalted oil (DAO).[5−9] Metallic compounds can be effectively enriched in the deoiled asphalt fraction (DOA) when they are separated on the basis of their solubility in a low-molecular-weight solvent (e.g., propane, butane, and pentane).[10] However, some metal porphyrin compounds still remain in the DAO because of the limited separation efficiency.[11,12]

Asphaltenes are the heavy oil fractions that are soluble in aromatic hydrocarbons, such as benzene and toluene; however, these compounds are insoluble in saturated hydrocarbons, such as *n*-pentane, *n*-hexane, and *n*-heptane.[13,14] The asphaltene molecules are composed of condensed aromatic rings linked with aliphatic chains and naphthenic rings. Asphaltenes include a large variety of chemical species containing sulfur, nitrogen, heavy metals, and functional groups, such as acids and bases. The presence of polar functional groups in asphaltenes confers these molecules with high surface activity, which may cause surface charges on their interfaces. This high surface activity accounts for its high adsorption onto metallic (e.g., gold or steel),[15,16] metal oxide (e.g., $Fe_2O_3$, $TiO_2$, and $Al_2O_3$), mineral (e.g., clay, calcite, and kaolin),[17] and metal oxide nanoparticle[18] surfaces.

The surface activity of asphaltene allows for the possible removal of DAO porphyrins by enhancing porphyrin adsorption onto the asphaltene surface. In this way, the asphaltene and porphyrin can be totally concentrated in DOA. The mechanism of this porphyrin–asphaltene interaction should be known to develop such a technology. However, the adsorption kinetics and thermodynamics of the interaction between porphyrins and asphaltene have not been reported to date.

In this paper, vanadyl porphyrin absorption on an asphaltene surface is studied using asphaltene from Canadian oil sands bitumen vacuum tower bottom (VTB) and vanadyl octaethylporphyrin (VO-OEP). The mechanisms for the adsorption kinetics and thermodynamics of this system were elucidated. The study provides information for enhancing the interaction between vanadyl porphyrins and asphaltene and increasing the removal ratio of metals in the deasphalting process.

## EXPERIMENTAL SECTION

**Materials and Preparations.** The asphaltene in this experiment was obtained from Canadian oil sands bitumen VTB from the commercial mining of oil sands bitumen by vacuum distillation at 524 °C. The $C_7$ asphaltene was prepared using the four-component analysis method (SH/T 0509-92) of residual oil from RIPP. The oil sample (1 g) was mixed with *n*-heptane (70 mL) and then heated under reflux for 1.5 h in a glycerol bath (120 °C). After which, the samples were filtered and the asphaltenes were left on the filter paper. Then, the filter paper refluxed using *n*-heptane for 3 h. Finally, the

Received: March 27, 2013
Revised: September 28, 2013
Published: September 29, 2013

   dx.doi.org/10.1021/ef400533t | *Energy Fuels* 2013, 27, 6408–6418

**Table 1. Specifications of VO-OEP**

| | |
|---|---|
| name | vanadyl octaethylporphyrin |
| appearance (color) | red to purple |
| molecular formula | $C_{36}H_{44}N_4OV$ |
| molecular weight | 599.71 |
| chemical family | vanadium complex |
| purity (%) | >99 |

filter paper was placed in a vacuum oven, dried at 120 °C under 93 ± 1 kPa for approximately 2 h, and weighed.

VO-OEP was obtained from J&K Scientific, Ltd., the specifications of which are shown in Table 1. This compound is structurally similar to vanadyl etioporphyrin (VO-ETIO; Figure 1). Toluene, *n*-heptane, and *n*-pentane were purchased from Beijing Chemical Works.

A UV-1201 ultraviolet−visible (UV−vis) spectrophotometer designed by Beijing Beifen-Ruili Analytical Instrument Corporation, Ltd. was used for the VO-OEP quantitative analysis. The YKKY HX-101 constant temperature water bath oscillator was procured from the Beijing Changliu Scientific Instrument Corporation, Ltd.

The asphaltenes before and after adsorption were analyzed by Transmission electron microscopy (TEM), Brunauer−Emmett−Teller (BET), and positive-ion electrospray ionization (ESI) Fourier transform ion cyclotron resonance mass spectrometry (FT-ICR MS). TEM graphs were obtained using a FEI Tecnai $G^2$ F20 field emission transmission electron microscope. The maximum acceleration voltage was 200 kV. The point resolution was 0.24 nm, and the information resolution was 0.14 nm. The surface area by BET adsorption of nitrogen was obtained using an automatic physical adsorption analyzer of surface area and porosity of American Quadrasorb SI. High-resolution MS data were obtained using a Bruker Apex 9.4 T FT-ICR mass spectrometer coupled with Apollo II ESI. The data were collected in 4M data sets.

**Adsorption Experiments.** The experimental process was the VTB asphaltene adsorbed porphyrin from pentane (the VTB asphaltene softening point was above 150 °C; therefore, this situation had implications of VTB asphaltene as solids). The study of the interaction between porphyrin and asphaltenes was determined by liquid−solid absorption. Meanwhile, to study the kinetic and thermodynamic mechanisms of vanadyl porphyrin adsorption onto the VTB asphaltene, the capacity of the VTB asphaltene to adsorb VO-OEP was measured and the corresponding adsorption isotherm was obtained.

On the basis of the solubility of VO-OEP in pentane, the standard solution was prepared by dissolving VO-OEP in pentane at different concentrations, namely, 2, 4, 6, 8, and 10 μg/mL. The absorbance of VO-OEP in the solution was then measured at the strong absorption peak wavelength (570 nm) using the UV−vis spectrophotometer. The standard VO-OEP curves in pentane were determined from these measurements. Thus, the unknown concentration of a pentane solution containing VO-OEP could be obtained on the basis of its absorbance.

*Selection of Dosage or Concentration.* The asphaltene dosage should depend upon the size of the adsorption equipment. Otherwise, some asphaltene would accumulate at the bottom of the container, or the change in absorbance would not be evident in the upper layer of the pentane solution with VO-OEP. Therefore, in this study, the dosage of asphaltene ranged from 0.01 to 0.05 g. Meanwhile, the high concentrations of the upper layer of the pentane solution with VO-OEP were preferred; these concentrations ranged from 10 to 15 μg/mL.

*Blank Experiment.* The prepared VTB asphaltene (0.5 g) was added to the pentane solution (20 mL) and then kept at 20 °C using a constant temperature vibrator (water bath) for ∼48 h. The asphaltene did not dissolve in the pentane solution and was precipitated to the bottom. The upper part of the pentane solution was clear and colorless, and its absorbance was measured using the UV−vis spectrophotometer. The results are shown in Figure 4a. The results showed there were no vanadyl porphyrins in the upper part of the pentane solution. This experiment proved that the vanadium in the asphaltenes cannot desorb from the pentane solution.

*Measurement of the Adsorption Kinetics.* The VTB asphaltene (0.01 or 0.02 g) was added to 3.5 mL of the VO-OEP pentane solution (10 or 15 μg/mL) and then kept at 20 °C using a constant temperature vibrator (water bath) for ∼30 h. The asphaltene did not dissolve in the VO-OEP pentane solution and was precipitated to the bottom. The absorbance of the upper part of the VO-OEP pentane solution was measured using the UV−vis spectrophotometer. The VO-OEP concentration was determined on the basis of the measured absorbance. The adsorption capacity of vanadyl porphyrins at different time points could be calculated using eq 1.

$$q_t = (C_0 - C_t)V/M \tag{1}$$

*Measurement of Adsorption Thermodynamics.* Asphaltene (0.05 g) was added to VO-OEP pentane solutions with different concentrations (4, 6, 8, 10, and 12 μg/mL). The mixtures were kept for 48 h in a constant temperature vibrator (water bath) at different temperatures (288, 293, and 298 K). The VO-OEP concentration of the upper part of the solution was measured using the UV−vis spectrophotometer. The equilibrium adsorption capacity of VO-OEP could be calculated using eq 2

$$q_e = (C_0 - C_e)V/M \tag{2}$$

where $C_0$ is the initial concentration of the adsorbate (mg/L), $C_t$ is the adsorbate concentration at a given time $t$ (mg/L), $C_e$ is the adsorbate equilibrium concentration (mg/L), $V$ is the solution volume (mL), and $M$ is the adsorbate dosage (g).

## THEORY

**Kinetic Models.** The experimental data were fitted to different kinetic models to investigate the adsorption mechanism. Data regarding the adsorption capacity and time were fitted to four kinetic models (pseudo-first-order, pseudo-second-order, Elovich, and diffusion kinetic models) to further study the adsorption dynamics of VO-OEP adsorbed onto asphaltene.

*Pseudo-first-Order Equation.* The pseudo-first-order equation is a common kinetic model for describing the simulation of a solid−liquid adsorption system.[19−21] This equation can be expressed as follows:

$$dq_t/dt = k_1(q_e - q_t) \tag{3}$$

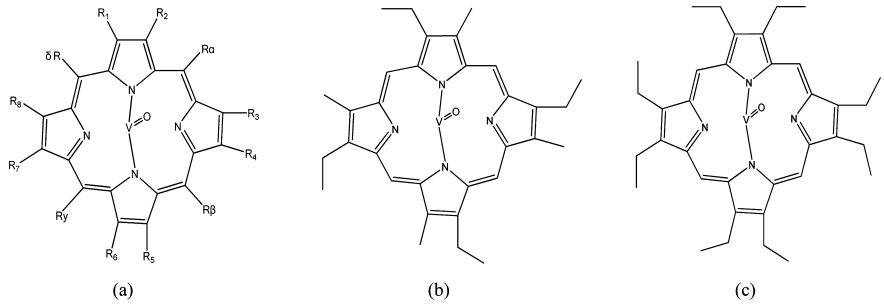


**Figure 1.** General structure of vanadyl porphyrins: (a) general vanadyl porphyrin structure, (b) VO-ETIO, and (c) VO-OEP.


dx.doi.org/10.1021/ef400533t | Energy Fuels 2013, 27, 6408−6418

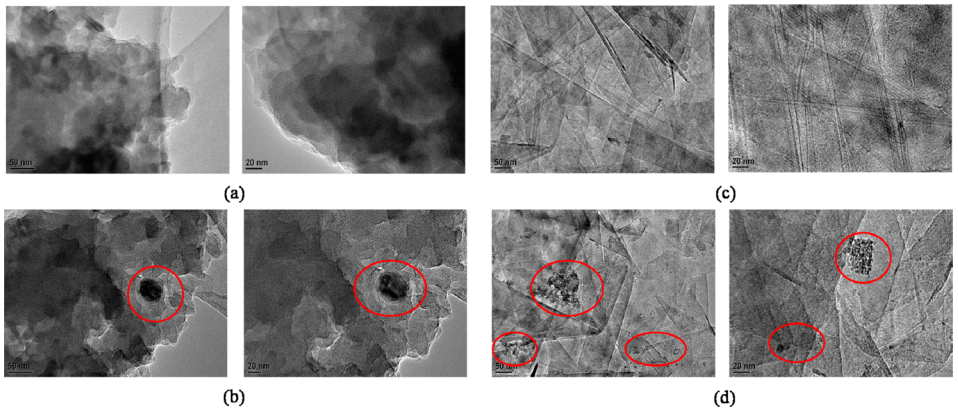


**Figure 2.** TEM images of asphaltene/graphene before and after adsorption: (a) asphaltene before adsorption, (b) asphaltene after adsorption, (c) graphene before adsorption, and (d) graphene after adsorption (50 and 20 nm).

The equation is integrated by applying the boundary conditions ($q_t = 0$ at $t = 0$, and $q_t = q_t$ at $t = t$). The pseudo-first-order equation can be expressed as

$$q_t = q_e(1 - e^{-k_1 t}) \tag{4}$$

where $q_e$ and $q_t$ are the amount of VO-OEP adsorbed (mg/g) onto the asphaltene surface at equilibrium and at time $t$, respectively, and $k_1$ is the rate constant of adsorption ($min^{-1}$) for the pseudo-first-order equation.

*Pseudo-second-Order Equation.* The pseudo-second-order equation is another common kinetic model for describing the simulation of solid–liquid adsorption systems.[22−24] This equation can be expressed as

$$dq_t/dt = k_2(q_e - q_t)^2 \tag{5}$$

The equation is integrated by applying the boundary conditions ($q_t = 0$ at $t = 0$, and $q_t = q_t$ at $t = t$). The pseudo-second-order equation is shown in eq 6

$$q_t = k_2 q_e^{\ 2} t/(1 + k_2 q_e t) \tag{6}$$

where $k_2$ is the adsorption rate constant (g $mg^{-1}$ $min^{-1}$) for the pseudo-second-order equation. $q_e$ and $k_2$ have higher values at high adsorption rates.

*Elovich Equation.* The Elovich equation is used to describe chemical adsorption onto a solid.[25−27] This equation is generally expressed as

$$dq_t/dt = Ae^{-Bq_t} \tag{7}$$

where $A$ is a constant that represents the initial adsorption rate (mg $g^{-1}$ $min^{-1}$) and $B$ is a rate constant, namely, the desorption constant (g/mg) during any experiment. The equation is integrated by applying the boundary conditions ($q_t = 0$ at $t = 0$, and $q_t = q_t$ at $t = t$). The equation becomes

$$q_t = \ln(1 + ABt)/B \tag{8}$$

To simplify the Elovich equation, in the case of $ABt \gg 1$, the equation becomes

$$q_t = \ln(AB)/B + \ln(t)/B \tag{9}$$

*Diffusion Kinetic Model.* Three steps are generally required for solute adsorption from liquidoid to solid particles. The first step is particle external diffusion, also known as liquid membrane diffusion. At this stage, the adsorbent in the liquid phase is spread through the fluid film on the surface of the adsorbent to the outer surface of the granules. The second step is particle internal diffusion, at which the adsorbent from the outer surface of the particle enters the center of the particle hole and spreads to the external surfaces. The final stage is the adsorption reaction. The total rate of the adsorption process is controlled by one of the slowest procedures in the entire process, which is the rate-determining step.

The diffusion kinetic model is the sum of the pore and surface diffusion.[28−30] This sum can be calculated from the following equation:

$$q_t = k_p t^{0.5} + C \tag{10}$$

where $C$ is the parameter of the internal diffusion model and $k_p$ is the rate constant of internal diffusion.

**Adsorption Isotherm.** Two adsorption isotherm equations were used in this study, namely, the Langmuir and Freundlich equations.[31−33] The experimental data at different temperatures should obey certain isotherms, which can be determined on the basis of the correlation coefficients of these equations. The error of the models can likewise be calculated using their correlation coefficients.

The Langmuir (eq 11) and Freundlich (eq 12) isotherms can be expressed by the following equations:

$$q_e = \frac{K_L q_{max} C_e}{1 + K_L C_e} \tag{11}$$

where $C_e$ is the equilibrium concentration ($\mu$g/mL), $q_e$ is the monolayer adsorption capacity ($\mu$g/g), and $K_L$ is the Langmuir constant (L/mg)

$$q_e = K_F C_e^{\ 1/n} \tag{12}$$

where $K_F$ is a constant indicating the adsorption capacity of the adsorbent ($\mu$g/g) and the constant $1/n$ indicates the intensity of the adsorption.

**Thermodynamic Study.** The thermodynamic parameters were used to evaluate the energy variation during the adsorption process and to assess if the process was spontaneous.[34−37] The thermodynamic parameters of adsorption are the change in standard free energy ($\Delta G°$; kJ/mol), enthalpy ($\Delta H°$; kJ/mol), and entropy ($\Delta S°$; kJ $mol^{-1}$ $K^{-1}$). The relationship among these parameters is expressed as

$$\Delta G° = \Delta H° - T\Delta S° \tag{13}$$


dx.doi.org/10.1021/ef400533t | *Energy Fuels* 2013, 27, 6408−6418

The individual parameters are determined using the following equations:

$$\Delta G^\circ = -RT \ln K \tag{14}$$

and

$$\ln K = \frac{\Delta S^\circ}{R} - \frac{\Delta H^\circ}{RT} \tag{15}$$

where $R$ is the universal gas constant (8.314 J mol$^{-1}$ K$^{-1}$) and $T$ is the temperature.

The feasibility of the process is reflected by the product of $\Delta G^\circ$ and $\Delta H^\circ$ and the value of $\Delta S^\circ$, which can be calculated from the slope and intercept of log $K$ versus $1/T$. The adsorption process is exothermic if the value of $\Delta H^\circ$ is negative. The disorder of the adsorption process at the solid−liquid interface is determined by the standard entropy.

## RESULTS AND DISCUSSION

**Adsorbent Characterization.** The prepared VTB asphaltene was placed in a *n*-pentane solution containing VO-OEP and kept in a constant temperature vibrator (water bath) at 20 °C for 48 h. After adsorption, the upper layer of the pentane solution with VO-OEP was removed and the asphaltene was left at the bottom. The asphaltene before and after adsorption were analyzed by TEM, BET, and positive-ion ESI FT-ICR MS.

The microscopic structure of asphaltene before and after adsorption can be clearly described by TEM. The TEM images of asphaltene and graphene before and after adsorption (50 and 20 nm) are shown in Figure 2. Graphene instead of asphaltene was used to run the same experiments because of the similarities of their aromatic structure. The structure of graphene is more clean and easy to identify the porphyrin adsorption. It can be clearly seen that, in both cases, black spots appeared after adsorption of porphyrin. This indicated that metal porphyrin was adsorpted on graphene on some areas. Therefore, the above conclusion about asphaltene could be proven.

The BET surface area is shown in Table 2. As shown in Table 2, the surface area of the asphaltene is very small and the surface area of the asphaltene before and after adsorption drops from 5.3 to 3.8 m$^2$/g. The trend indicated that a certain amount of porphyrins was absorbed on the asphaltene. Of course, this small difference seems not a strong proof on porphyrin adsorption.

**Table 2. Surface Area of Asphaltenes before and after Adsorption by BET**

| name of sample | BET surface area (m$^2$/g) |
|---|---|
| asphaltene | 5.3 |
| asphaltene + V | 3.8 |

The FT-ICR MS results are shown in Figure 3, with the mass spectrum of $C_{36}H_{44}N_4OV$. After the adsorption of Canadian VTB asphaltene, the peak can also be observed. The result indicated that a certain amount of VO-OEP was absorbed on the VTB asphaltene, thereby confirming the adsorption process between asphaltene and VO-OEP again.

The adsorption experiments were conducted in a constant temperature vibrator (water bath) at 20 °C. The asphaltene dosage was 0.01 g, and the initial concentration of the pentane solution containing VO-OEP was 10 μg/mL. During the adsorption of VO-OEP onto VTB asphaltene, the upper layer of the solution was sampled at different time points. A typical spectrum of the upper layer exhibits several characteristics, as analyzed by UV−vis and shown in Figure 4b. The plot of $C_t$ versus $t$ is shown in Figure 4c.

As shown in Figure 4b, three peaks (570, 530, and 410 nm) were always present in the UV−vis spectra of VO-OEP. The peak at 410 nm is called the Soret peak. The peaks at 570 and 530 nm are referred to as the $\alpha$ and $\beta$ peaks, respectively, which are the characteristic absorption peaks for VO-OEP. Meanwhile, the absorbance of VO-OEP at 570 nm was reduced with an increasing adsorption time, thereby indicating that the VO-OEP concentration in the upper layer of the solution was decreased. Therefore, the amount of VO-OEP adsorbed on the asphaltene was increased. The adsorption finally reached equilibrium when the concentration of the upper layer of the solution no longer varied over time (Figure 4c). The decreasing VO-OEP concentration in the solution revealed the effectiveness of the adsorption process, which agreed with the positive-ion ESI FT-ICR MS results.

**Adsorption Rate and Adsorption Kinetics.** The effect of the adsorbent amount, initial adsorbate concentration, and temperature on the amount of VO-OEP adsorbed (mg/g) on asphaltene was investigated. The kinetic adsorption data were processed to understand the dynamics of the adsorption process.

*Effects of the Adsorption Dosage.* The influence of asphaltene dosage on the adsorption process was investigated at 20 °C, using 15 μg/mL pentane solution containing VO-OEP. The results are shown in Figure 5a.

The equilibrium amount of adsorbed VO-OEP increased from 2.26 to 4.68 mg/g for asphaltene as the adsorption dosage was decreased from 0.02 to 0.01 g. In contrast, the overall trends of the two curves were similar for different dosages of asphaltene. Three sections were observed on every curve. In the first section ($t$ < 200 min), the change in slope of the curve was notably high and the adsorption capacity increased rapidly. The rate of adsorption was relatively fast, thereby indicating that a rapid physical process occurs at the beginning of the adsorption process. On the second section (200 < $t$ < 750 min), the change in slope of the curve was distinctly slow and the rate of adsorption decreased with the time increased. On the third section ($t$ > 750 min), the line plot was nearly constant and the adsorption was said to be in equilibrium until the amount of adsorption no longer varied over time. However, the total adsorption time was relatively long. Thus, approximately 1800 min were necessary to reach adsorption equilibrium.

The pseudo-first-order, pseudo-second-order, Elovich, and diffusion kinetic models were selected for fitting the experimental data in Figure 5a to describe the adsorption process. The results are shown in panels b and c of Figure 5, and the fitting parameters are shown in Table 3.

The fitting results of four kinetic models showed that the correlation coefficients of the pseudo-first- and pseudo-second-order equations are higher than those of the Elovich and diffusion equations. Meanwhile, in comparison to the $q_{e,cal}$ of the pseudo-second-order equation, the $q_{e,cal}$ of the pseudo-first-order equation is close to $q_{e,exp}$. Therefore, the entire adsorption process was well-described by the pseudo-first-order equation. In addition, the rate constant of adsorption ($k_1$) for the pseudo-first-order equation increased with the increasing asphaltene dosage. This trend was caused by the increased availability of the combining sites for VO-OEP and asphaltene when the asphaltene dosage was increased. Therefore, vanadyl porphyrins and asphaltene require less time to combine with each other.


dx.doi.org/10.1021/ef400533t | Energy Fuels 2013, 27, 6408−6418

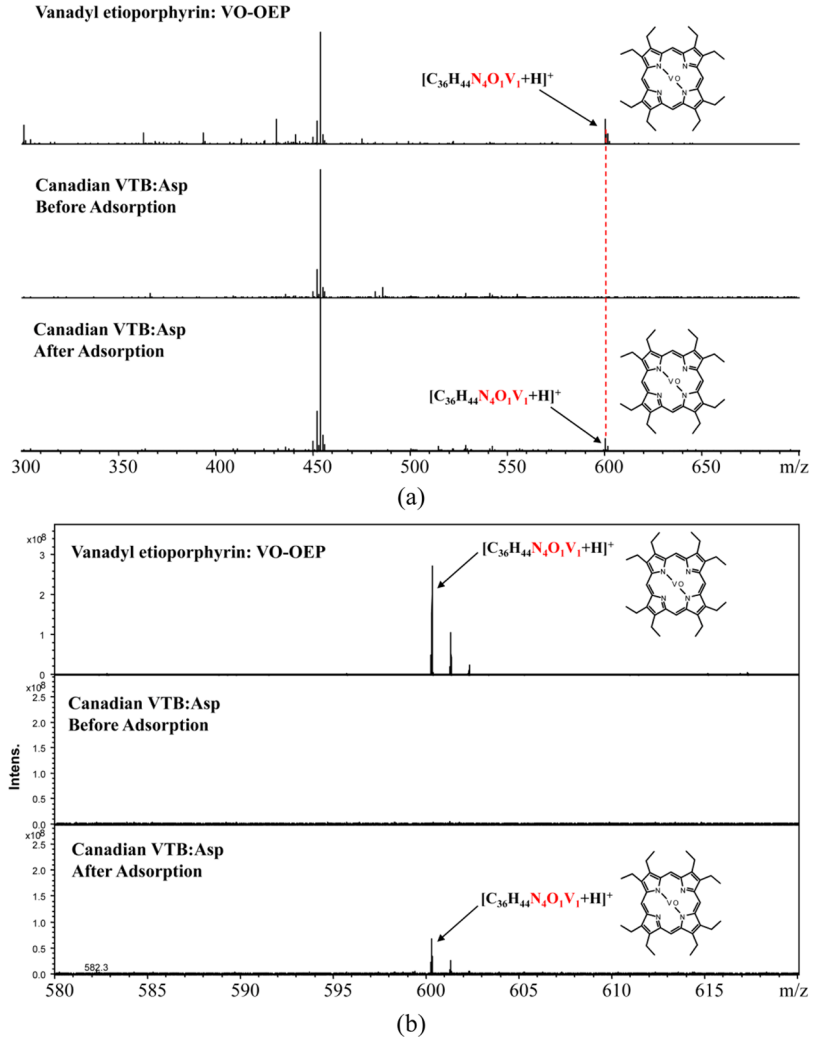


**Figure 3.** Positive-ion ESI FT-ICR mass spectra of VO-OEP and Canadian bitumen VTB asphaltene before and after adsorption.

The trend of $k_1$ to change with the adsorbent dosage agrees with that in other adsorption systems reported in the literature. For example, Demirbas et al.[27] studied the adsorption of Cu(II) ions from aqueous solutions using hazelnut shell activated carbon (HSAC). During adsorption, the rate constant of adsorption ($k_1$) for the pseudo-first-order equation increased with adsorbent dosage.

*Effects of the Initial Adsorbate Concentration.* The influence of the concentration of the pentane solutions containing VO-OEP on the adsorption process was likewise investigated at 20 °C, with an asphaltene dosage of 0.01 g. The results are shown in Figure 6a. Changing the initial concentration of VO-OEP solution from 10 to 15 $\mu$g/mL caused the equilibrium amount adsorbed to increase from 3.25 to 4.68 mg/g. The overall trend of the two curves was similar to that of the curves in Figure 5a.

After analysis of the effects of the adsorption dosage to the adsorption process, the pseudo-first- and pseudo-second-order kinetic models were selected to describe the adsorption process by fitting them to the experimental data in Figure 6a. The results are shown in panels b and c of Figure 6. The fitting parameters are summarized in Table 4.

Results showed that both of the correlation coefficients of the pseudo-first- and pseudo-second-order equations were very high. The correlation coefficient of the pseudo-first-order equation was slightly higher than that of the pseudo-second-order equation (0.995 and 0.992, respectively). Meanwhile, in comparison to the $q_{e,cal}$ of the pseudo-second-order equation, the $q_{e,cal}$ of the pseudo-first-order equation is close to $q_{e,exp}$. Therefore, the entire adsorption process was well-described by the pseudo-first-order equation. In addition, the rate constant of adsorption ($k_1$) decreased as the VO-OEP concentration in pentane increased. On the one hand, this trend was attributed to the increased probability of collisions in the molecule as the VO-OEP concentration rose. On the contrary, the probability of collision between vanadyl porphyrins and asphaltenes decreased. Consequently, combining vanadyl porphyrins and asphaltenes would require more time. On the other hand, from the TEM images of VO-OEP adsorbed on asphaltene, VO-OEP was adsorbed on some areas. Repetitious adsorption on some areas would cause the aggregation of VO-OEP on asphaltene. Then, the aggregation will become more serious with $C_0$ increasing ($q_e$ increased with $C_0$ increasing). This kind of aggregation leads to the decreasing of $k_1$. In addition, the tendency of $k_1$ to change with the concentration agrees with other adsorption systems reported in the literature.[27,38] For example, Ahmad et al. studied the adsorption behavior of $\beta$-carotene on a silica-based adsorbent. $\beta$-Carotene solutions with initial concentrations of 50−300 mg/L were prepared with *n*-hexane. The rate constant of adsorption ($k_1$) for the pseudo-first-order equation decreased as the concentration increased.


dx.doi.org/10.1021/ef400533t | *Energy Fuels* 2013, 27, 6408−6418

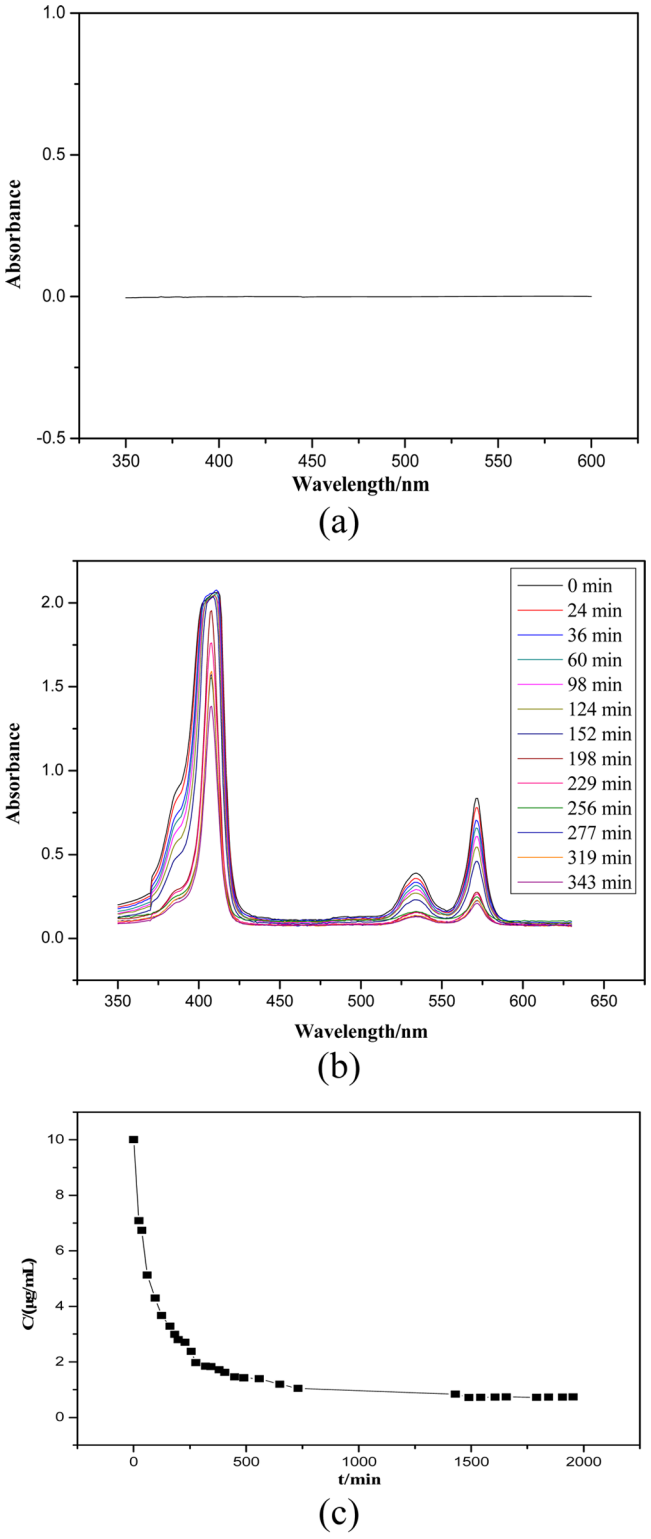


**Figure 4.** UV−vis spectra of the (a) upper solution at the blank experiment and (b) upper solution at the adsorption experiment and (c) VO-OEP concentration calculated from the signal intensity at different time points.

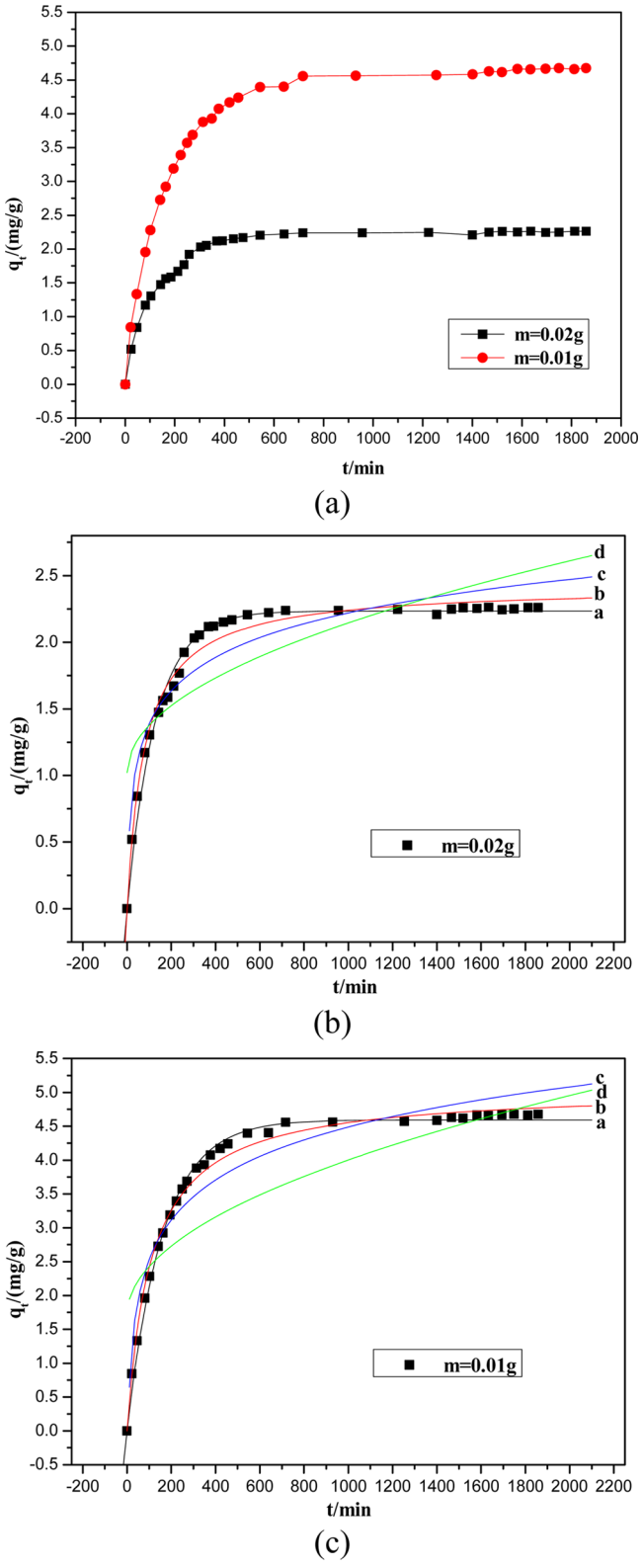


**Figure 5.** (a) Plot of $q_t$ as a function of the adsorption time at different asphaltene dosages ($m$). (b and c) Adsorption kinetics at different asphaltene dosages (a, plots of the pseudo-first-order equation; b, plots of the pseudo-second-order equation; c, plots of the Elovich equation; and d, plots of the diffusion equation).

*Effects of the Temperature.* The influence of the temperature on the adsorption process was investigated for 15 $\mu$g/mL pentane solutions containing VO-OEP, with an asphaltene dosage of 0.01 g. The results are presented in Figure 7a. The equilibrium adsorption capacity of VO-OEP increased from 4.56 mg/g at 298 K to 4.96 mg/g at 288 K, with the adsorption capacity decreasing with the rising temperature. The trend of the three curves at different temperatures was similar to that of the curves in Figure 5a.


dx.doi.org/10.1021/ef400533t | *Energy Fuels* 2013, 27, 6408−6418

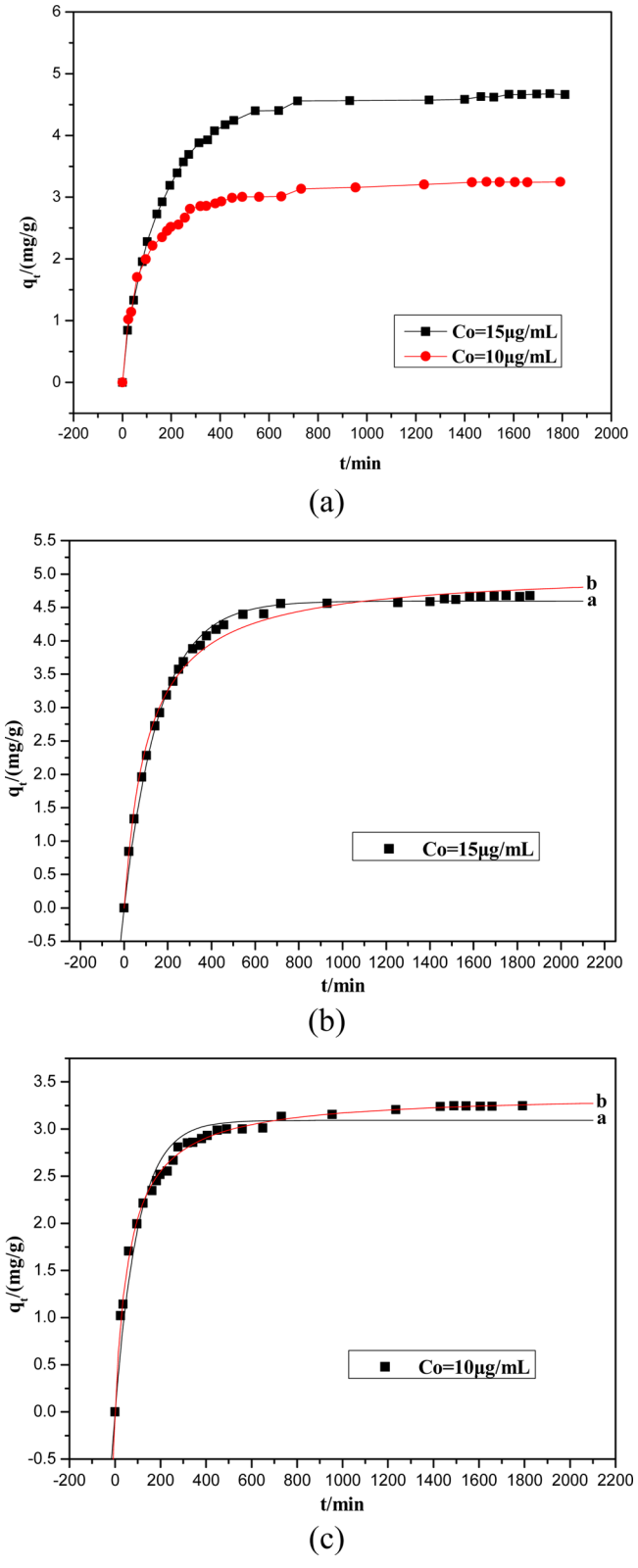


**Figure 6.** (a) Plot of $q_t$ as a function of the adsorption time at different initial VO-OEP concentrations ($C_0$). (b and c) Adsorption kinetics at different initial concentrations (a, plots of the pseudo-first-order equation; b, plots of the pseudo-second-order equation).

After analysis of the effects of the adsorption dosage and the initial adsorbate concentration to the adsorption process, the pseudo-first- and pseudo-second-order kinetic models were selected to describe the adsorption process by fitting them to the experimental data in Figure 7a. The results are shown in panels b–d of Figure 7. The fitting parameters are outlines in Table 5. Results showed that the entire adsorption process was well-described by the pseudo-first-order equation, which agreed with the effects of adsorption dosage and initial adsorbate concentration results. In addition, the rate constant of adsorption ($k_1$) for the pseudo-first-order equation slightly increased with the temperature.

**Adsorption Isotherms.** The isotherm equations of Langmuir and Freundlich were selected for fitting the experimental data to describe the adsorption process between VO-OEP and asphaltene. The results are shown in Figure 8. The fitting parameters are shown in Table 6.

The experimental data from different temperatures fitted well to both adsorption isotherm equations, as shown in Table 6. The correlation coefficient of the Freundlich isotherm was higher than that of the Langmuir isotherm (0.999 and 0.995, respectively). The Freundlich isotherm is an empirical model, which assumes that the activities of the adsorption sites are different, while the Langmuir isotherm is a classic monolayer adsorption model. The high correlation coefficients of both models suggest that the adsorption process is complicated. In some areas, the adsorption process is monolayer adsorption, while in other areas, the adsorption process is multilayer adsorption. The multilayer adsorption could cause the aggregation of VO-OEP on asphaltene on some areas. Therefore, it is easy to understand the reason of aggregation. In addition, the constant $K_F$ indicates the adsorption capacity of the adsorbent ($\mu$g/g). The adsorption capacity decreases as the temperature increases, thereby indicating that the value of $K_F$ at low temperatures is higher than that at high temperatures. The change in $1/n$ follows an opposite trend. The constant $1/n$ indicates the intensity of the adsorption. The value of $1/n$ decreases as the temperature increases, as shown in Table 6. Therefore, the intensity of the adsorption is weak at high temperatures.

**Adsorption Thermodynamics.** The $K_F$ calculated from the Freundlich model can be used in eq 14 to determine the value of $\Delta G°$. The other thermodynamic parameters ($\Delta H°$ and $\Delta S°$) can be calculated using eq 15. Therefore, the plot of ln $b$ versus $1/T$ should indicate a linear relationship with a slope of $-\Delta H°/R$ and an intercept of $\Delta S°/R$. The plot of ln $b$ versus $1/T$ and the corresponding thermodynamic parameters are shown in Figure 9 and Table 6, respectively.

All of the values of $\Delta G°$ for the adsorption process between VO-OEP and asphaltenes are negative, as shown in Table 6. Therefore, the process is spontaneous. Moreover, the absolute value of $\Delta G°$ is less than 20 kJ/mol. The absolute value of $\Delta G°$ decreases as the temperature increases, thereby indicating that low-temperature conditions favor the adsorption process between vanadyl porphyrins and asphaltenes better than high-temperature conditions. To some extent, the value of $\Delta G°$ can reflect that the process is chemistry or physical adsorption.[39] The $\Delta G°$ of chemistry adsorption is from −400 to −80 kJ mol$^{-1}$. The $\Delta G°$ of physical adsorption is from −20 to 0 kJ mol$^{-1}$. Thus, there exist physical adsorption between porphyrins and asphaltene in the adsorption process.

Furthermore, $\Delta H°$ is negative, which suggests an exothermic process. The absolute value of $\Delta H°$ is greater than 40 kJ/mol. This value demonstrates the strong interaction between VO-OEP and asphaltene. In addition, the enthalpy change during the adsorption process is ∼50 kJ/mol, which is significantly


dx.doi.org/10.1021/ef400533t | Energy Fuels 2013, 27, 6408–6418

**Table 3. Fitting Parameters of the Adsorption Kinetics Equations**

| | pseudo-first-order equation $q_t = q_e(1 - e^{-k_1 t})$ | | | pseudo-second-order equation $q_t = (k_2 q_e^2 t)/(1 + k_2 q_e t)$ | | | |
|---|---|---|---|---|---|---|---|
| $m$ (g) | $q_{e,cal}$ (mg/g) | $k_1$ ($min^{-1}$) | $R^2$ | $q_{e,cal}$ (mg/g) | $k_2$ (g $mg^{-1}$ $min^{-1}$) | $R^2$ | $q_{e,exp}$ (mg/g) |
| $m$ = 0.01 | 4.594 | 0.00620 | 0.995 | 5.054 | 0.00179 | 0.992 | 4.676 |
| $m$ = 0.02 | 2.235 | 0.00773 | 0.987 | 2.421 | 0.00512 | 0.983 | 2.261 |
| | Elovich equation $q_t = 1/B \ln(AB) + \ln(t)/B$ | | | diffusion equation $q_t = k_p t^{0.5} + C$ | | | |
| $m$ (g) | $B$ (g/mg) | $A$ (mg $g^{-1}$ $min^{-1}$) | $R^2$ | $k_p$ (mg $g^{-1}$ $min^{-0.5}$) | $C$ (mg/g) | $R^2$ | |
| $m$ = 0.01 | 1.170 | 0.163 | 0.940 | 0.0827 | 1.703 | 0.723 | |
| $m$ = 0.02 | 2.750 | 0.163 | 0.907 | 0.0356 | 1.021 | 0.630 | |

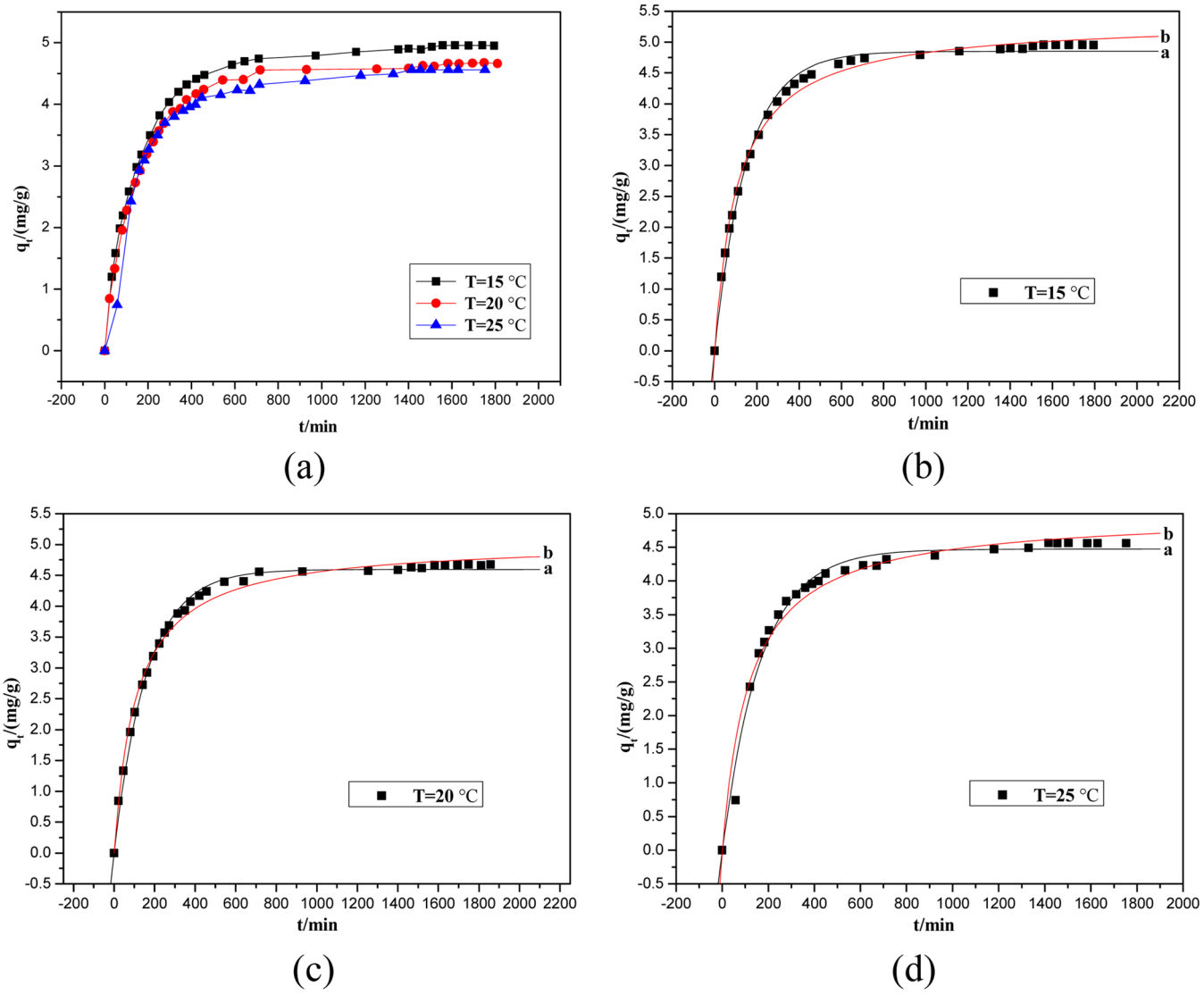


**Figure 7.** (a) Plot of $q_t$ as a function of the adsorption time at different temperatures ($T$). (b–d) Adsorption kinetics at different temperatures (a, plots of the pseudo-first-order equation; b, plots of the pseudo-second-order equation).

**Table 4. Fitting Parameters of the Adsorption Kinetics Equations**

| | pseudo-first-order equation $q_t = q_e(1 - e^{-k_1 t})$ | | | pseudo-second-order equation $q_t = (k_2 q_e^2 t)/(1 + k_2 q_e t)$ | | | |
|---|---|---|---|---|---|---|---|
| $C_0$ ($\mu$g/mL) | $q_{e,cal}$ (mg/g) | $k_1$ ($min^{-1}$) | $R^2$ | $q_{e,cal}$ (mg/g) | $k_2$ (g $mg^{-1}$ $min^{-1}$) | $R^2$ | $q_{e,exp}$ (mg/g) |
| $C_0$ = 15 | 4.594 | 0.00620 | 0.995 | 5.054 | 0.00179 | 0.992 | 4.676 |
| $C_0$ = 10 | 3.092 | 0.00991 | 0.960 | 3.374 | 0.00460 | 0.996 | 2.261 |

larger than that of hydrogen bonding (5–30 kJ/mol).[40] This result suggests that a strong secondary bond exists between porphyrin and asphaltene (probably a metal-coordination interaction). The identification of the secondary bond type requires further investigation. Taking into consideration $\Delta G°$ and $\Delta H°$, there are both chemistry and physical adsorptions between porphyrins and


dx.doi.org/10.1021/ef400533t | Energy Fuels 2013, 27, 6408–6418

**Table 5. Fitting Parameters of the Adsorption Kinetics Equations**

| | pseudo-first-order equation $q_t = q_e(1 - e^{-k_1 t})$ | | | pseudo-second-order equation $q_t = (k_2 q_e^2 t)/(1 + k_2 q_e t)$ | | | |
|---|---|---|---|---|---|---|---|
| $T$ (°C) | $q_{e,cal}$ (mg/g) | $k_1$ ($min^{-1}$) | $R^2$ | $q_{e,cal}$ (mg/g) | $k_2$ (g $mg^{-1}$ $min^{-1}$) | $R^2$ | $q_{e,exp}$ (mg/g) |
| 15 | 4.850 | 0.00596 | 0.992 | 5.358 | 0.0017 | 0.994 | 4.956 |
| 20 | 4.594 | 0.00620 | 0.995 | 5.054 | 0.00179 | 0.992 | 4.676 |
| 25 | 4.473 | 0.00651 | 0.982 | 5.001 | 0.00168 | 0.967 | 4.562 |

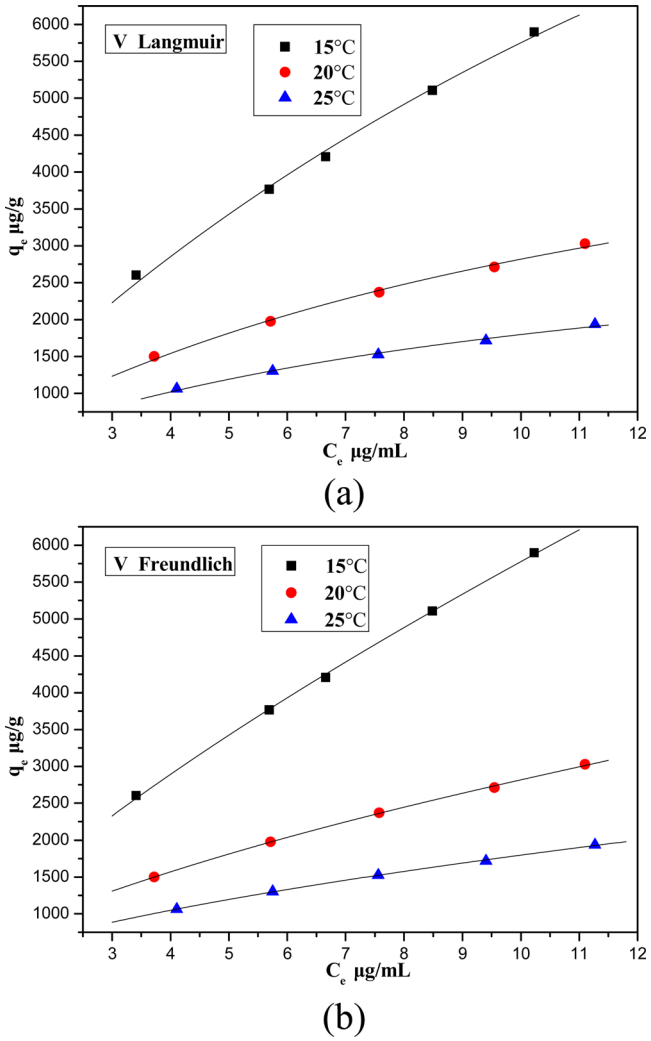


**Figure 8.** (a) Langmuir and (b) Freundlich isotherms.

asphaltene in the adsorption process. It is speculated that there are both monolayer and multilayer adsorption between asphaltene and VO-OEP. The same conclusion can be drawn for the adsorption isotherm. In addition, the disorder of the adsorption process at the solid−liquid interface is determined by standard entropy. The larger the degree of disorder, the greater the standard entropy. When vanadyl porphyrins were transferred from the free state to the more ordered adsorbed state, the value of $\Delta S°$ is negative.

From the results of adsorption kinetics, it is found that the initial rate and equilibrium adsorption amount of adsorption is related to the asphaltene content, temperature, and concentration of porphyrin. The initial rates regressed by first-order equation show that the lower ratio of porphyrin to asphaltene and higher temperature favor a high initial rate. However, the change is not so significant. The equilibrium adsorption amount of porphyrin changes significantly. The higher ratio of porphyrin to asphaltene and lower temperature favor a high

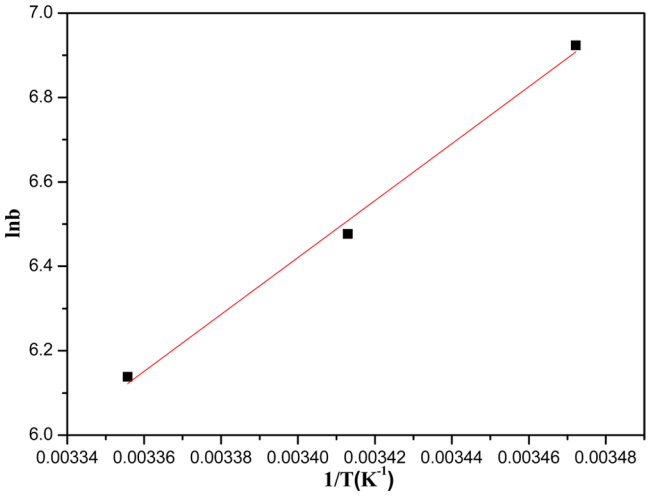


**Figure 9.** van't Hoff plot of VO-OEP.

**Table 6. Isotherms and Thermodynamic Parameters**

| | Langmuir isotherm | | | Freundlich isotherm | | |
|---|---|---|---|---|---|---|
| $T$ (°C) | $q_{max}$ (mg/g) | $K_L$ (L/mg) | $R^2$ | $K_F$ | $1/n$ | $R^2$ |
| 15 | 17.858 | 0.0475 | 0.995 | 1.016 | 0.755 | 0.999 |
| 20 | 6.303 | 0.0809 | 0.995 | 0.650 | 0.637 | 0.999 |
| 25 | 3.661 | 0.0965 | 0.993 | 0.463 | 0.588 | 0.999 |
| | | | $\Delta G°$ (kJ/mol) | | | |
| $\Delta H°$ (kJ/mol) | $\Delta S°$ (J/mol) | | 288 K | 293 K | 298 K | |
| −56.07 | −137.26 | | −16.58 | −15.78 | −15.21 | |

adsorption capacity. From the results of adsorption thermodynamics, it is found that the adsorption process is spontaneous and exothermic. There are both chemistry and physical adsorptions between two porphyrins and asphaltene in the adsorption process. In the future, the adsorption interaction should be enhanced using some methods. Anyway, this research is a fundamental one. The study will provide information for enhancing the interaction between vanadyl porphyrins and asphaltene and increasing the removal ratio of metals in the deasphalting process.

## CONCLUSION

An interaction between VO-OEP and VTB asphaltene was observed in this study. A certain amount of VO-OEP was absorbed onto the VTB asphaltene, thereby supporting the adsorption process between asphaltene and VO-OEP. Adsorption between VO-OEP and asphaltene was affected by the asphaltene dosage, the concentration of the pentane solution containing VO-OEP, and the temperature. However, the overall trends of these plots (the adsorption capacity versus time) were highly similar. The adsorption rate was initially extremely fast. The adsorption rate became much slower, and equilibrium was established after around 1800 min. A comparison of the kinetic models for the overall adsorption rate showed that the adsorption process can be


dx.doi.org/10.1021/ef400533t | Energy Fuels 2013, 27, 6408−6418

well-described by the pseudo-first-order equation. The isotherm study indicated that the adsorption equilibrium can be fitted by the Freundlich isotherm. The thermodynamic parameters related to the adsorption process were evaluated. Furthermore, when the experimental data and the various spectra are analyzed, a strong interaction between porphyrin and asphaltene was confirmed.

## AUTHOR INFORMATION


### Corresponding Author

*Telephone: +8610-8973-9015. E-mail: sqzhao@cup.edu.cn and/or zhaosuoqi@gmail.com.


### Notes

The authors declare no competing financial interest.

## ACKNOWLEDGMENTS

This work was supported by the National "Twelfth Five-Year" Plan for Science and Technology Support (2012BAE05B06) and the National Natural Science Foundation of China (NSFC) (U1162204 and 21176254).

## REFERENCES


(1) Dechaine, G. P.; Gray, M. R. Chemistry and association of vanadium compounds in heavy oil and bitumen, and implications for their selective removal. *Energy Fuels* **2010**, *24* (5), 2795−2808.

(2) Qian, K. N.; Edwards, K. E.; Mennito, A. S.; Walters, C. C.; Kushnerick, J. D. Enrichment, resolution, and identification of nickel porphyrins in petroleum asphaltene by cyclograph separation and atmospheric pressure photoionization Fourier transform ion cyclotron resonance mass spectrometry. *Anal. Chem.* **2010**, *82* (1), 413−419.

(3) McKenna, A. M.; Purcell, J. M.; Rodgers, R. P.; Marshall, A. G. Identification of vanadyl porphyrins, in a heavy crude oil and raw asphaltene by atmospheric pressure photoionization Fourier transform ion cyclotron resonance (FT-ICR) mass spectrometry. *Energy Fuels* **2009**, *23* (4), 2122−2128.

(4) Barwise, A. J. G.; Whitehead, E. V. Separation and structure of petroporphyrins. *Phys. Chem. Earth* **1980**, *12*, 181−192.

(5) Oden, E. C.; Foret, E. L. Deasphalting crude residuum for catalytic cracker. Commercial production using horizontal setters and propane solvent. *Ind. Eng. Chem.* **1950**, *42* (10), 2088−2095.

(6) Al-Sabawi, M.; Seth, D.; de Bruijn, T. Effect of modifiers in *n*-pentane on the supercritical extraction of Athabasca bitumen. *Fuel Process. Technol.* **2011**, *92* (10), 1929−1938.

(7) Wu, J. Y.; Dabros, T. Process for solvent extraction of bitumen from oil sand. *Energy Fuels* **2012**, *26* (2), 1002−1008.

(8) Brons, G.; Yu, J. M. Solvent deasphalting effects on whole cold lake bitumen. *Energy Fuels* **1995**, *9* (4), 641−647.

(9) Cao, F. H.; Jiang, D.; Li, W. D.; Du, P. A.; Yang, G. Z.; Ying, W. Y. Process analysis of the extract unit of vacuum residue through mixed C4 solvent for deasphalting. *Chem. Eng. Process.* **2010**, *49* (1), 91−96.

(10) Freeman, D. H.; Swahn, I. D.; Hambright, P. Spectrophotometry and solubility properties of nickel and vanadyl porphyrin complexes. *Energy Fuels* **1990**, *4* (6), 699−704.

(11) Long, J.; Shen, B. X.; Ling, H.; Zhao, J. G.; Lu, J. C. Novel solvent deasphalting process by vacuum residue blending with coal tar. *Ind. Eng. Chem. Res.* **2011**, *50* (19), 11259−11269.

(12) Samano, V.; Guerrero, F.; Ancheyta, J.; Trejo, F.; Diaz, J. A batch reactor study of the effect of deasphalting on hydrotreating of heavy oil. *Catal. Today* **2010**, *150* (3−4), 264−271.

(13) Liao, Z. W.; Zhou, H. G.; Graciaa, A.; Chrostowska, A.; Creux, P.; Geng, A. Adsorption/occlusion characteristics of asphaltenes: Some implication for asphaltene structural features. *Energy Fuels* **2005**, *19* (1), 180−186.

(14) Bouhadda, Y.; Bormann, D.; Sheu, E.; Bendedouch, D.; Krallafa, A.; Daaou, M. Characterization of Algerian Hassi-Messaoud asphaltene structure using Raman spectrometry and X-ray diffraction. *Fuel* **2007**, *86* (12−13), 1855−1864.

(15) Abdallah, W. A.; Taylor, S. D. Surface characterization of adsorbed asphaltene on a stainless steel surface. *Nucl. Instrum. Methods Phys. Res., Sect. B* **2007**, *258* (1), 213−217.

(16) Rudrake, A.; Karan, K.; Horton, J. H. A combined QCM and XPS investigation of asphaltene adsorption on metal surfaces. *J. Colloid Interface Sci.* **2009**, *332* (1), 22−31.

(17) Dean, K. R.; McAtee, J. L., Jr. Asphaltene adsorption on clay. *Appl. Clay Sci.* **1986**, *1* (4), 313−319.

(18) Nassar, N. N.; Hassan, A.; Luna, G.; Pereira-Almao, P. Kinetics of the catalytic thermo-oxidation of asphaltenes at isothermal conditions on different metal oxide nanoparticle surfaces. *Catal. Today* **2013**, *207*, 127−132.

(19) Erdem, M.; Ozverdi, A. Kinetics and thermodynamics of Cd(II) adsorption onto pyrite and synthetic iron sulphide. *Sep. Purif. Technol.* **2006**, *51* (3), 240−246.

(20) Tarley, C.; Andrade, F. N.; de Santana, H.; Zaia, D.; Beijo, L. A.; Segatelli, M. G. Ion-imprinted polyvinylimidazole−silica hybrid copolymer for selective extraction of Pb(II): Characterization and metal adsorption kinetic and thermodynamic studies. *React. Funct. Polym.* **2012**, *72* (1), 83−91.

(21) Azouaou, N.; Sadaoui, Z.; Djaafri, A.; Mokaddem, H. Adsorption of cadmium from aqueous solution onto untreated coffee grounds: Equilibrium, kinetics and thermodynamics. *J. Hazard. Mater.* **2010**, *184* (1−3), 126−134.

(22) Eftekhari, S.; Habibi-Yangjeh, A.; Sohrabnezhad, S. Application of AlMCM-41 for competitive adsorption of methylene blue and rhodamine B: Thermodynamic and kinetic studies. *J. Hazard. Mater.* **2010**, *178* (1−3), 349−355.

(23) Venkatesha, T. G.; Viswanatha, R.; Arthoba Nayaka, Y.; Chethana, B. K. Kinetics and thermodynamics of reactive and vat dyes adsorption on MgO nanoparticles. *Chem. Eng. J.* **2012**, *198−199*, 1−10.

(24) Chen, G. C.; Shan, X. Q.; Zhou, Y. Q.; Shen, X. E.; Huang, H. L.; Khan, S. U. Adsorption kinetics, isotherms and thermodynamics of atrazine on surface oxidized multiwalled carbon nanotubes. *J. Hazard. Mater.* **2009**, *169* (1−3), 912−918.

(25) Khaled, A.; El Nemr, A.; EI-Sikaily, A.; Abdelwahab, O. Removal of Direct N Blue-106 from artificial textile dye effluent using activated carbon from orange peel: Adsorption isotherm and kinetic studies. *J. Hazard. Mater.* **2009**, *165* (1−3), 100−110.

(26) Aydin, Y. A.; Aksoy, N. D. Adsorption of chromium on chitosan: Optimization, kinetics and thermodynamics. *Chem. Eng. J.* **2009**, *151* (1−3), 188−194.

(27) Demirbas, E.; Dizge, N.; Sulak, M. T.; Kobya, M. Adsorption kinetics and equilibrium of copper from aqueous solutions using hazelnut shell activated carbon. *Chem. Eng. J.* **2009**, *148* (2−3), 480−487.

(28) Sheela, T.; Nayaka, Y. A.; Viswanatha, R.; Basavanna, S.; Venkatesha, T. G. Kinetics and thermodynamics studies on the adsorption of Zn(II), Cd(II) and Hg(II) from aqueous solution using zinc oxide nanoparticles. *Powder Technol.* **2012**, *217*, 163−170.

(29) Albadarin, A. B.; Mangwandi, C.; Al-Muhtaseb, A. H.; Walker, G. M.; Allen, S. J.; Ahmad, M. Kinetic and thermodynamics of chromium ions adsorption onto low-cost dolomite adsorbent. *Chem. Eng. J.* **2012**, *179*, 193−202.

(30) Ngah, W.; Hanafiah, M. Adsorption of copper on rubber (*Hevea brasiliensis*) leaf powder: Kinetic, equilibrium and thermodynamic studies. *Biochem. Eng. J.* **2008**, *39* (3), 521−530.

(31) Kuo, C. Y.; Wu, C. H.; Wu, J. Y. Adsorption of direct dyes from aqueous solutions by carbon nanotubes: Determination of equilibrium, kinetics and thermodynamics parameters. *J. Colloid Interface Sci.* **2008**, *327* (2), 308−315.

(32) Wang, H. L.; Fei, Z. H.; Chen, J. L.; Zhang, Q. X.; Xu, Y. H. Adsorption thermodynamics and kinetic investigation of aromatic amphoteric compounds onto different polymeric adsorbents. *J. Environ. Sci. (Beijing, China)* **2007**, *19* (11), 1298−1304.

(33) Ding, L.; Deng, H. P.; Wu, C.; Han, X. Affecting factors, equilibrium, kinetics and thermodynamics of bromide removal from aqueous solutions by MIEX resin. *Chem. Eng. J.* **2012**, *181*, 360−370.

(34) Wu, C. H. Adsorption of reactive dye onto carbon nanotubes: Equilibrium, kinetics and thermodynamics. *J. Hazard. Mater.* **2007**, *144* (1−2), 93−100.
(35) Uzun, I.; Guzel, F. Kinetics and thermodynamics of the adsorption of some dyestuffs and *p*-nitrophenol by chitosan and MCM−chitosan from aqueous solution. *J. Colloid Interface Sci.* **2004**, *274* (2), 398−412.
(36) Anirudhan, T. S.; Radhakrishnan, P. G. Thermodynamics and kinetics of adsorption of Cu(II) from aqueous solutions onto a new cation exchanger derived from tamarind fruit shell. *J. Chem. Thermodyn.* **2008**, *40* (4), 702−709.
(37) Theydan, S. K.; Ahmed, M. J. Adsorption of methylene blue onto biomass-based activated carbon by $FeCl_3$ activation: Equilibrium, kinetics, and thermodynamic studies. *J. Anal. Appl. Pyrolysis* **2012**, *97*, 116−122.
(38) Ahmad, A. L.; Chan, C. Y.; Shukor, S.; Mashitah, M. D. Adsorption kinetics and thermodynamics of *β*-carotene on silica-based adsorbent. *Chem. Eng. J.* **2009**, *148* (2−3), 378−384.
(39) Jaycock, M. J.; Parfitt, G. D. *Chemistry of Interfaces*; Ellis Horwood, Ltd.: Chichester, U.K., 1981; pp 12−13.
(40) Jeffrey, G. A. *An Introduction to Hydrogen Bonding*; Oxford University Press: New York, 1997; Vol. *12*.